Am J Clin Exp Urol 2023;11(4):293-303
www.ajceu.us /ISSN:2330-1910/AJCEU0148844

Original Article

EZH2 and matrix co-regulate phenotype and KCNB2 expression in bladder smooth muscle cells

Priyank Yadav[1,2], Tabina Ahmed[1], Suejean Park[1], Martin Sidler[3], Annette Schröder[4], Karen J Aitken[1], Darius Bägli[1,5]

[1]The Hospital for Sick Children, Toronto, Ontario, Canada; [2]Department of Urology and Renal Transplantation, Sanjay Gandhi Postgraduate Institute of Medical Sciences, Lucknow, Uttar Pradesh, India; [3]Paediatric and Neonatal Surgery, Klinikum Stuttgart, Stuttgart, Baden-Württemberg, Germany; [4]Department of Urology and Pediatric Urology of The University Medical Center Mainz, Mainz, Rheinland-Pfalz, Germany; [5]Division of Urology, Department of Surgery, University of Toronto, Toronto, Ontario, Canada

Received December 29, 2022; Accepted May 17, 2023; Epub August 15, 2023; Published August 30, 2023

Abstract: Background: Partial bladder outlet obstruction (PBO) is a widespread cause of urinary dysfunction and patient discomfort, resulting in immense health care costs. Previously, we found that obstruction is associated with altered regulation of epigenetic machinery and altered function. Here we examined if PBO and chronic bladder obstructive disease (COBD) affect epigenetic marks in a proof of principle gene and explored mechanisms of its epigenetic regulation using *in vitro* models. Methods: Archival obstruction tissues from COBD had been created in 200-250 g female Sprague-Dawley rats by surgical ligation of the urethra for 6 weeks, followed by removal of the suture and following animals for 6 more weeks. Obstruction (PBO) is the 6-week ligation only. Sham ligations comprise passing the suture behind the urethra. Histone3 lysine27 trimethylation (H3K27me3) was studied by immunostaining and Chromatin immunoprecipitation (ChIP)/PCR. The interaction of matrix with KCNB2 regulation was studied in human bladder SMC plated on damaged matrix and native collagen and treated with vehicle or UNC1999. Cells were analyzed by immunostaining for cell phenotype, and western blotting for KCNB2, H3K27me3 and EZH2. Effects of conditioned media from these cells were also examined on cell phenotype. siRNA against KCNB2 was examined for effects on cell phenotype and gene expression by RT-qPCR. Results: H3K27me3 increased by immunofluorescence during PBO, and by ChIP/PCR during COBD in the CpG Island (CGI) as well as 350 bp upstream. Obstruction vs. sham also showed an increase in H3K27me3 deposition. In SMC *in vitro*, EZH2 inhibition restored KCNB2 expression and partially restored SMC phenotype. Conclusions: Regulation of KCNB2 at the promoter demonstrated dynamic changes in H3K27me3 during COBD and obstruction. *In vitro* models suggest that matrix plays a role in regulation of EZH2, H3K27me3 and KCNB2, which may play a role in the regulation of smooth muscle phenotype *in vivo*.

Keywords: Bladder obstruction, potassium channels, epigenetics, matrix biology, smooth muscle, H3K27me3

Introduction

Partial bladder obstruction (PBO) is a condition in which there is an obstruction to the flow of urine from the bladder, leading to incomplete bladder emptying, and primarily affects 50% of elderly men who suffer from diseases such as prostate hyperplasia [1-3]. This can result in a range of symptoms, including frequent urination, difficulty urinating and weak urine flow. The diagnosis of PBO typically involves a combination of medical history, physical examination, and diagnostic tests. Laboratory tests may include a urinalysis to check for signs of infection or inflammation, uroflowmetry to assess the urine flow, as well as blood tests to assess kidney function. Imaging tests such as ultrasound or cystoscopy may also be used to visualize the bladder and assess the degree of obstruction. Patients with PBO may experience symptoms such as urinary hesitancy, dribbling, or retention, as well as discomfort or pain in the lower abdomen or pelvic region, otherwise known as lower urinary tract symptoms (LUTS) and complications, such as frequency, urgency, nocturia, and urinary incontinence [1, 2]. There may also be an increased risk of bladder stones or urinary tract infections. The treatment of PBO

depends on the underlying cause and severity of the obstruction. Mild cases may be managed with medication, such as alpha-blockers, which relax the smooth muscle of the bladder and urethra, allowing for better urine flow. More severe cases may require surgical intervention, such as transurethral resection of the prostate or bladder neck incision, to remove the obstruction.

With appropriate management, most patients can expect to experience a significant improvement in symptoms and quality of life. However, in cases where the obstruction is left untreated, there is a risk of complications such as chronic kidney disease or bladder damage.

Indeed, PBO induces structural and functional bladder remodeling and is distinguished by the establishment of an inflammatory response, smooth muscle hypertrophy, accumulation of the extracellular matrix (ECM) [4, 5], and later, a decompensation of the bladder itself [2, 6, 7].

Previous research conducted by our laboratory has shown DNA methylation to be a key player in the pathophysiology and downstream signaling of PBO, due to its effects on the genetic expression of certain obstruction-induced growth factors [8]. Matrix in particular was seen to augment expression of DNA methyltransferase enzymes and modify SMC phenotype through epigenetic mechanisms [9]. In addition, DNA methylation inhibition alters the genetic expression of brain-derived neurotrophic factor (BDNF), both *in vitro* and *in vivo*, increasing its expression during PBO while decreasing particular isoforms during de-obstruction (or Chronic obstructive bladder disease or COBD) [8, 10]. In turn, the expression of specific BDNF variants associates with specific pathophysiologic changes in the bladder.

However, one gene KCNB2 was consistently downregulated during both obstruction and COBD [8, 10], but the mechanisms and downstream consequences of this are relatively unknown.

While DNA methylation is a key epigenetic mechanism in gene silencing and gene regulation in response to environmental cues [9, 11, 12], histone 3 lysine 27 trimethylation (H3K27me3) is another major mechanism of epigenetic gene repression. Enhancer of Zest Homologue 2 (EZH2) is the main catalytic enzyme in the polycomb repressive complex 2 (PRC2) contributing to H3K27me3. In development and UTI models, EZH2 is known to play a crucial role in urothelial growth and differentiation [13, 14]. EZH2 or PRC2 activity has been associated with matrix production and remodeling in other diseases [15-17]. Here we examined the interaction of H3K27me3 deposition and matrix on KCNB2 expression during PBO and COBD, and SMC marker expression.

Methods

Partial bladder outlet obstruction and de-obstruction of animal models, and bladder pathophysiology readings

Archival adult female (200 to 250 g, 10 to 12 weeks old) Sprague-Dawley rats (Charles River Laboratories, Wilmington, MA) had been randomized into either PBO, COBD or sham groups as illustrated in Supplementary Figure 1 [10, 18]. PBO and COBD underwent the same surgical procedure that involved ligation of the urethra at the level of the bladder neck using a silk tie over a 0.9 mm rod to ensure that the urethra was not obliterated. Shams underwent a control surgery where the suture was passed behind the urethra, but not tied. PBO, COBD and shams were followed for 6 weeks, the timeline in which bladder obstruction developed, and were assessed for bladder pathophysiology (e.g., voiding patterns, bladder mass, residual volumes, bladder efficiency). The animals were kept in a housing area maintained between 20-26°C, with a relative humidity of 40-70%, the lighting set on a 12-hour light/dark cycle, minimum noise and adequate ventilation. After 6 weeks, COBD and shams underwent de-obstruction surgery that involved removal of the previously tied silk suture for COBD and simple open and closure of previous wound for shams, and were followed for another 6 weeks in the release phase (allowing for manifestation of COBD in the respective group), while PBO rat bladders were harvested. After the 6-week release period, bladder pathophysiology assessments were carried out, after which bladders were harvested within 1-2 days from the COBD and sham groups. Sample numbers for each treatment group are as follows: PBO = 8, COBD = 16, sham (12W) = 9. Bladder pathophysiology analysis was performed in a metabolic cage set-up and measured with *LoggerPro* software

version 3.9 (Vernier Software & Technology, Beaverton, OR) to confirm changes consistent with obstruction on non-invasive urodynamics in PBO and COBD animals (see Supplementary Table 1 for the archival subset) [8, 10]. The animal care committee of The Hospital for Sick Children Research Institute approved this study.

Culture on native and heat-denatured collagen and treatments

Glass-bottomed multi-well plates were coated with 2.3 mg/mL heat-denatured type I bovine collagen (Elastin products company, Owensville, MO). Matrices were equilibrated in EMEM (Wisent, ST-BRUNO, Québec) with antibiotic/antimycotic (Wisent) without serum prior to plating cells onto the gels. Cells were plated on denatured collagen (DNC) at a density of 5×10^3 cells/mL on 96 well plates or 1×10^4 cells/mL on 24 well plates in 2% fetal calf serum (Wisent) for 2 hours prior to addition of vehicle (DMSO), UNC1999 (1 μM, Tocris, Abingdon, United Kingdom), or GSK J4 (0.4 μM, Tocris) over an additional 46 hours. For Western experiments, cells were also plated on native type I collagen gels that were generated by neutralizing the collagen in 10 mM NaOH in 1X PBS, then incubating at 37°C.

RNA isolation, cDNA synthesis and real-time qPCR

RNA was isolated using the *miRNeasy Mini Kit* (Qiagen, Hilden, Germany), with bladder homogenization steps performed at 4°C using a refrigerated *Bullet Blender* (Next Advance, Troy, NY), and steel 0.3 to 1.5 mmol/L pellets for several 5-minute intervals at setting 8. RNA quality and quantity were measured using the *Nanodrop 2000/2000c* program, and also by Agilent BioAnalyzer (TCAG Department, Hospital for Sick Children, Toronto, Canada). cDNA synthesis from RNA samples was performed using the *qScript cDNA Synthesis Kit* (QuantaBio, Beverley, MA), and cDNA quality/quantity was measured using the Nanodrop 2000/2000c. SsoAdvanced Universal SYBR Green Supermix (Biorad, Hercules, CA) or AzuraView GreenFast qPCR Blue Mix (Froggabio, Toronto, Ontario) were utilized for amplification of 2 uL of cDNA or genomic DNA (in ChIP/PCR) at the temperatures indicated in the Supplementary Table 2. Several reference genes were utilized for optimal normalization through the ΔΔCt method, as previously [8] (See Supplementary Table 2 notes). Primers for EZH2, BDNF, CTGF and KCBN2 (Supplementary Table 2) were used for Real-time qPCR analysis of the cDNA samples on the *ViiA 7 Real-Time PCR System* and software (Thermofisher, Waltham, MA). The ΔΔCt analysis of the results was carried out by normalization against the reference genes. Percentage input and fold-enrichment analysis of the genomic BDNF and KCNB2 profiles was performed for ChIP/PCR.

Immunofluorescent staining and confocal microscopy

As performed in previous literature [8], bladder cryosections or bladder smooth muscle cells (bSMC) were fixed in 4% paraformaldehyde (VWR, Mississauga, Ontario), washed in PBS three times, permeabilized by 0.2% Triton-X100 for 10 minutes, washed again and blocked (Block = 1 mg/mL BSA, 5% normal goat serum, 5% normal donkey serum (Jackson Immunolabs, West Grove, PA), 0.1% Tween 20, 1X PBS). Primary antibodies were added in block overnight at 4°C for the following: H3 Lysine 27 trimethylation (H3K27me3, *Active Motif,* Carlsbad, CA), smooth muscle actin (SMA or ACTA2, Sigma-Aldrich, St. Louis, MO), DNMT3a, Fibronectin1 (FN1, Sigma-Aldrich), calponin (Proteintech, San Diego, CA), potassium voltage-gated channel subfamily B member 2 (KCNB2, Alomone, Haifa, Israel), phospho-serine 1 myosin light chain (ser1-MLC, ECM Biosciences, Versailles, KY). After washing 3 times in 1XPBS, secondary antibodies were added in block as indicated in Figure legends (Alexa-488-donkey anti-rabbit, Cy3-donkey anti-mouse, Alexa-647-donkey-anti-rabbit, cross-absorbed Fab', Jackson Immunolabs), washed and stained for nuclei with 4',6-diamidino-2-phenylindole (DAPI, Sigma-Aldrich). Immunostaining was visualized on a spinning confocal microscope (*Olympus IX81*), equipped with a *Hamamatsu* camera, spectral borealis lasers. Micrographs were analyzed with the *Volocity* software (ver. 6.2, Perkin-Elmer, Waltham, MA) for measuring intensity and counting DAPI positive cells as the number of nuclei.

Western blotting

As performed in previous research [8], cells from collagen gels were lysed in 0.1% Triton

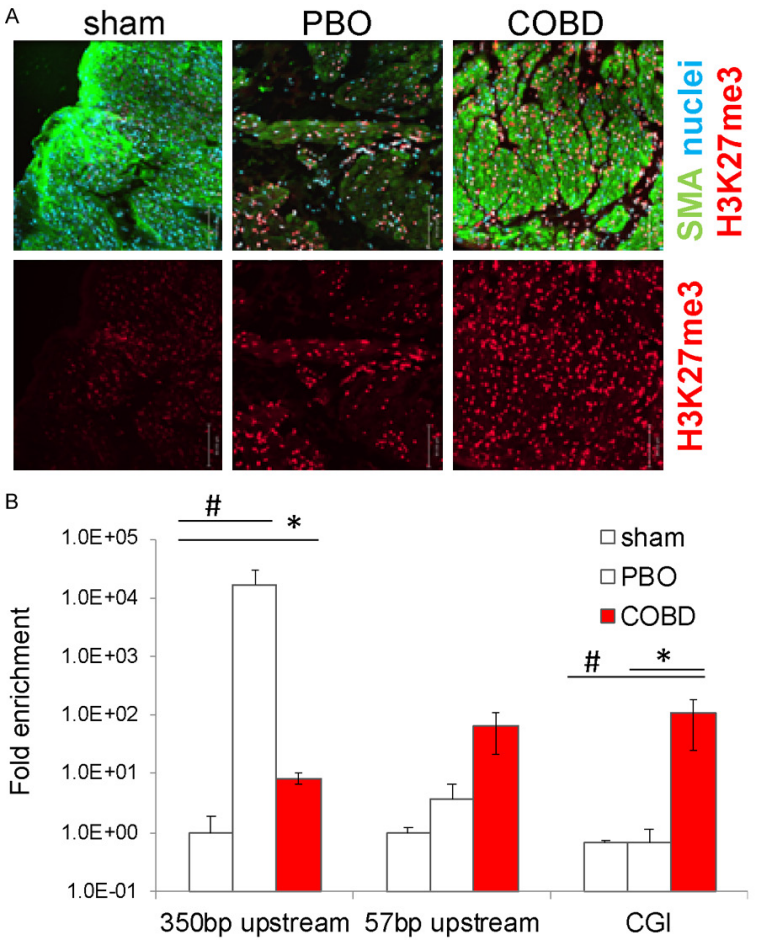

Figure 1. H3K27me3 nuclear intensity and expression profiles for *KCNB2 and BDNF* genes in Sham, PBO and COBD bSMC states. A. Immunofluorescent staining of bladder smooth muscle tissue was performed for analysis of detrusor region ACTA2 and H3K27me3 expression profiles in Sham, PBO and COBD. PBO tissue demonstrates a loss of ACTA2 expression, but a slight increase in H3K27me3 deposition compared to Sham tissue. COBD states show similar expression of SMA to Sham, but increased expression of H3K27me3 in comparison to PBO tissue. White bar = 90 microns. B. Fold-enrichment analysis of H3K27me3 ChIP/PCR fold enrichment in the upstream, downstream and CGI genomic regions of KCNB2, across Sham, PBO and COBD tissue states. There is a significant increase in H3K27me3 deposition in the CGI and 350 bp upstream regions in COBD vs. sham. PBO bladder tissue was also increased in H3K27me3 deposition in the region 350 bp upstream, by 1-tailed t-test. While in the 57 bp upstream region, both PBO and COBD tissue had higher H3K27me3 deposition though due to the variability of this increase it was not significant. #, one-tailed t-test, P<0.05; 2-tailed t-test, *, P<0.05.

X-100 with PBS and protease inhibitors. This was followed by quantification of cell and tissue lysates using the Pierce protein quantification kit (Thermofisher). 10-50 ug of protein were electrophoresed in 8-10% polyacrylamide gels, and electro blotted onto PVDF membranes. Membranes were blocked in Bovine serum albumin plus Skim milk (both from Bioshop, Burlington, Ontario, Canada) and incubated with primary antibodies for H3K27me3, EZH2 (Cell Signaling Technology, Danvers, MA), KCNB2 (Alamone), Fibronectin 1 (FN1, Proteintech) or pan-Actin (Sigma-Aldrich). After washing in TBST, blots were incubated with the secondary anti-rabbit or anti-mouse antibodies, conjugated to HRP (Cell Signaling Technology). Blots were developed using ECL and ECL chemiluminescent film (GE Healthcare, Little Chalfont, United Kingdom). Autoradiographs were scanned and analyzed on Image J.

Statistical analysis

The data was expressed as means (barplots) or median with quartiles values (box and whisker plots). Analysis of variance was performed prior to *post hoc* t-tests, with $P<0.05$ considered significant, on R software (version 4.1.3) with the 'stats' package (see Supplementary Materials). Where PCR values spanned over a logarithmic scale, ΔΔCt sample values were utilized for analysis of variance and *post hoc* t-tests. Where distribution was not normal, a *post hoc* non-parametric Kruskal's t-test was utilized. Where variances were unequal, Welch's t-test was performed (R scripts for the specific analysis methods provided in Supplementary Materials). The mean ± SE are presented in the text.

Results

H3K27me3 nuclear intensity increases during PBO and COBD, alongside changes in H3K-27me3 deposition at KCNB2

By immunostaining, H3K27me3 intensity in the nucleus of smooth muscle cells was increased in PBO and COBD vs. sham (**Figure 1A**). By ChIP/PCR, H3K27me3 marks, at the promoters of a highly downregulated gene KCNB2 [10,

18], were differentially methylated during both COBD and PBO (**Figure 1B**). H3K27me3 deposition increased during both PBO and COBD in the region 350 bp upstream of the CGI, whereas the H3K27me3 in the CGI remained higher only in COBD, $P<0.05$ vs. sham or PBO. At 57 bp upstream, variability in H3K27me3 resulted in only trends in increased deposition in COBD and PBO. ChIP/PCR for H3K27me3 deposition in an upregulated gene, BDNF, showed a mild decrease in COBD but not PBO (Supplementary Figure 2).

FN1 deposition increased in the detrusor during PBO and COBD vs. sham

Both PBO and COBD have been associated with changes in the matrix [19] and phenotype of the bladder smooth muscles, including loss of differentiation markers such as SERCA2, MYH11-SMB and myocardin [20-23]. Therefore, we examined FN1 and ACTA2 expression by immunostaining of sham, PBO and COBD cryosections. We found a significant increase in FN1 deposition in the muscle regions of the bladder during both PBO and COBD compared to sham (**Figure 2A**, **2B**). FN1 distribution in the detrusor appears to increase not only around the bundles but also within muscle bundles of the detrusor region. We then examined if FN1 expression in bladder SMC could be regulated by the downregulation of KCNB2 which we previously saw [8, 10, 18], or its related gene KCNB1, by siRNA depletion. KCNB2 depletion led to a significant increase in FN1 mRNA expression, $P<0.05$ (**Figure 2C**).

Matrix-regulated EZH2 activity alters KCNB2 expression and smooth muscle phenotype

As altered matrix is commonly found in both obstruction and COBD, and causes de-differentiation of bladder SMC [9, 19, 24], we examined if damaged matrix affects expression of KCNB2. KCNB2 expression decreased in human SMC plated on damaged collagen matrix (DNC) compared to native collagen (NC), by immunofluorescence and western (**Figure 3A**, **3B**; Supplementary Figure 3). Calponin staining also decreased in SMC on denatured collagen (**Figure 3**). We inhibited trimethylation and demethylation of H3K27 with pharmacologic agents, UNC1999 and GSK J4, respectively. UNC1999 treatment augmented KCNB2 expression on damaged matrix (**Figure 3A**, **3B**), although its effect on NC was reversed. Compared to native collagen, damaged matrix upregulated both H3K27me3 levels and EZH2 expression (**Figure 3A**, **3C**), which were decreased by the inhibitor UNC1999 (**Figure 3A**). Damaged matrix also increased EZH2 mRNA expression compared to native collagen gels. In contrast, GSK J4 treatment, which inhibits demethylase activity at H3K27 (promoting retention of repressive marks), did not have any effect on KCNB1/2 expression compared to vehicle, although it also increased calponin expression (**Figure 3B**).

EZH2 and H3K27me3 activity affected cell phenotype and KCNB2 expression

On denatured collagen matrix, which is analogous to the interstitial tissue of the bladders with PBO and COBD, the expression of H3K27me3 as well as its methylator EZH2 was high and the expression of KCNB2 was low (**Figure 3A**). Addition of EZH2 inhibitor UNC1999 not only suppressed EZH2 and H3K27me3 but also rescued KCNB2 (**Figure 3A**, **3B**). Similarly, UNC1999 was also associated with increased expression of calponin and cell hypertrophy (**Figure 3B**). DNC vs. native collagen also led to an increase in EZH2 mRNA expression (**Figure 3C**).

Conditioned media from DNC-plated cells contained FN1

As fibronectin secreted by SMC can be modulated by the microenvironment [25, 26], we assessed FN1 in the media of DNC treated cells. FN1 levels in the conditioned media of cells plated on damaged matrix were higher than in conditioned media from NC-plated cells (**Figure 4A**, Supplementary Figure 3). FN1 deposition could also be clearly visualized around cells plated on DNC vs. NC (**Figure 4B**).

Conditioned media from DNC-plated cells altered SMC phenotype

As our previous work demonstrated a role for damaged matrix (DNC) in SMC differentiation [9, 24], we tested if the CM from DNC vs. NC-plated cells could cause de-differentiation in naive cells plated on native collagen. Consistent with previous work, DNC vs. NC induced an increase in both cell counts and staining intensity of an acontractile marker, phosphoserine-1-MLC (**Figure 4C**). When we added CM from DNC-plated cells to naive cells on native

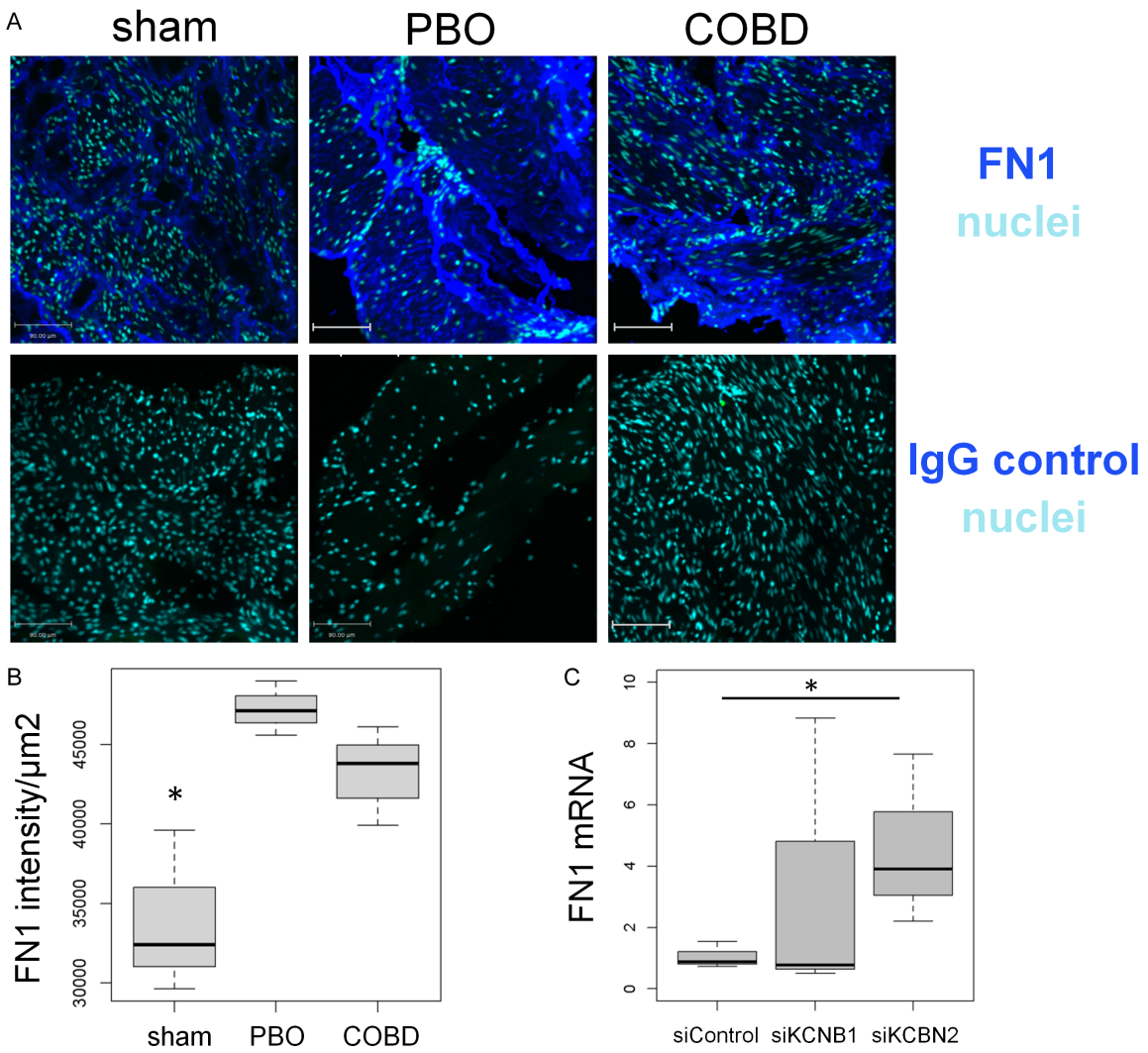

Figure 2. Effect of KCNB2 (siRNA) on FN1 expression. A. Immunofluorescent staining of bladder smooth muscle tissue for analysis of FN1 deposition in control, PBO, and COBD samples upon KCNB2 siRNA and BDNF treatments. FN1 expression in PBO states is significantly increased compared to Sham tissue, and also demonstrates bladder smooth muscle cell (bSMC) hypertrophy amongst the tissue. White bar for FN1+nuclei and nuclei stains = 90 microns. B. Intensity analysis for FN1 deposition per µm^2. Staining for FN1 was most intense in PBO tissues. COBD tissue also shows a significant increase in FN1 expression. However, in COBD tissues show slightly less expression of FN1 and less bSMC hypertrophy than PBO tissues. C. KCNB2 siRNA increases FN1 deposition human bladder smooth muscle cells (*, P<0.05).

collagen, this DNC-CM also increased cell counts above NC-CM treatment of naive cells on NC. DNC-CM effects on NC-plated naïve cells were not significantly different from DNC veh cells (plated on DNC without any added CM) in cell counts and staining intensity.

FN1 secretion into conditioned media of DNC-plated cells depended on EZH2 activity

UNC1999, the inhibitor of EZH2 activity, prevented the secretion of FN1 into media from cells plated on damaged matrix (**Figure 4D**). Expression levels of FN1 were low and similar with and without UNC1999 in cells plated on NC matrix.

KCNB2 dependent gene expression revealed reciprocal control of EZH2 gene expression

While EHZ2 activity played a role in decreasing KCNB2 expression, we examined if KCNB2 could in turn affect EZH2 expression. Using siRNA KCNB2 depletion, we found that down-regulation of KCNB2 but not KCNB1 elevated EZH2 mRNA expression, P<0.05 (**Figure 4E**).

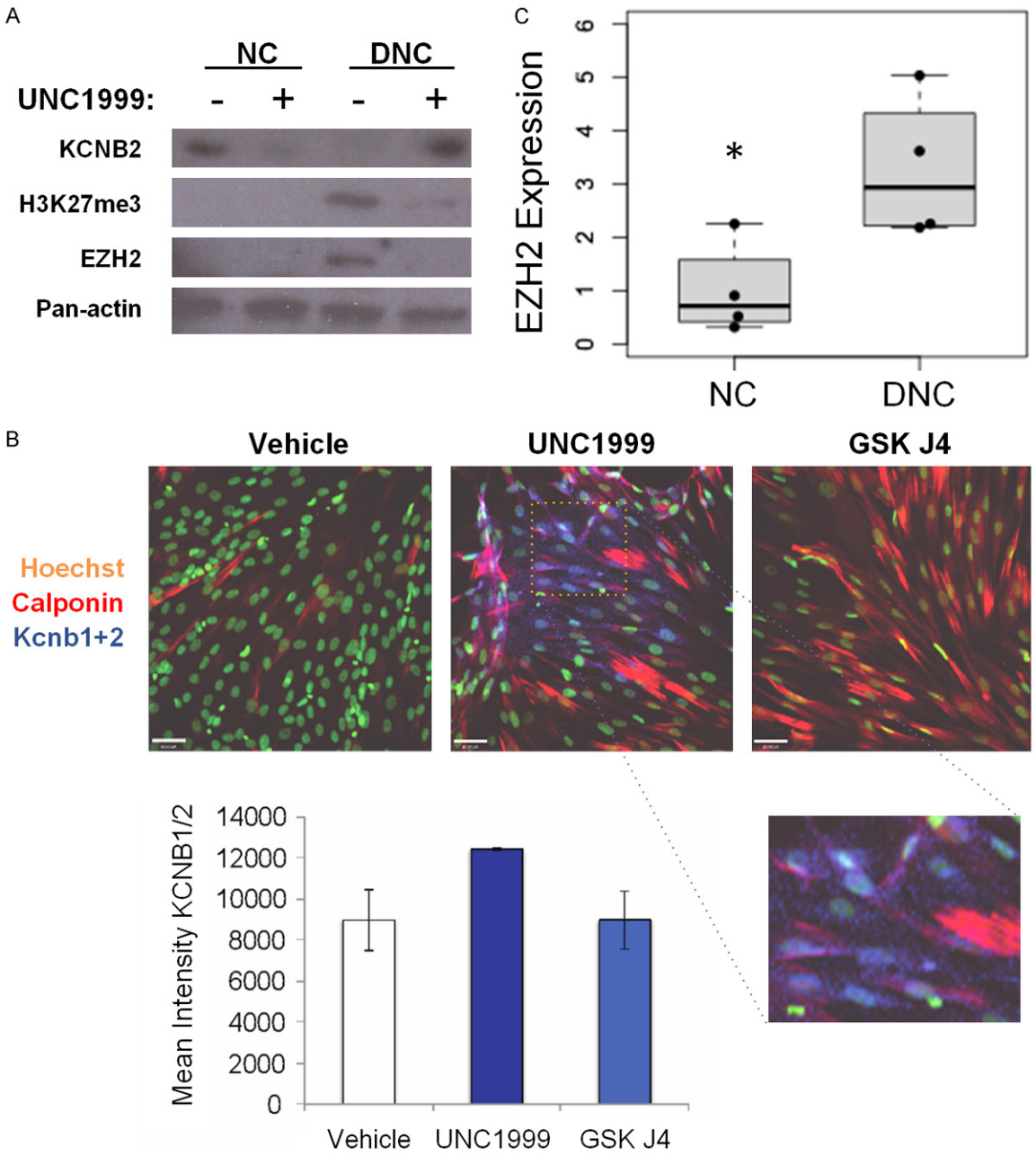

Figure 3. Damaged matrix increased EZH2 expression and H3K27 trimethylation while reducing KCNB2 expression and SMC differentiation. A. Western blotting for EZH2, H3K27me3 and KCNB2 in native collagen (NC) matrix and damaged (denatured) matrix (DNC) matrix upon UNC1999 treatment, with pan-actin expression as the control, showed that KCNB2 expression in SMC on NC is diminished upon addition of UNC1999 treatment, whereas expression H3K27me3 and EZH2 expression remains unchanged. However, the DNC matrix demonstrates an absence of H3K27me3 and EZH2 expression upon UNC1999 treatment, with a recovery of KCNB2 expression. B. Bladder smooth muscle cells plated on DNC were stained immunofluorescently for KCNB2 and Calponin expression in vehicle, UNC1999 treatment (EZH2 inhibition/H3K27me3 suppression), and GSK J4 treatment (H3K27me3 demethylase inhibition). Vehicle treatment demonstrates no expression of KCNB2, as well as minimal expression of Calponin and relatively small cell size. In contrast, UNC1999 treatment demonstrates significantly increased expression of KCNB2 and cell hypertrophy. While the GSK J4 treatment shows similar KCNB2 expression levels as Vehicle, cell hypertrophy as shown through the elongated cells also appears increased in comparison to UNC1999 treatment. White bar for Vehicle, UNC1999 and GSK J4 stains = 90 microns. KCNB1/2 expression (per field μm^2) in each treatment. C. Relative EZH2 transcription in SMC plated on DNC vs. NC are increased.

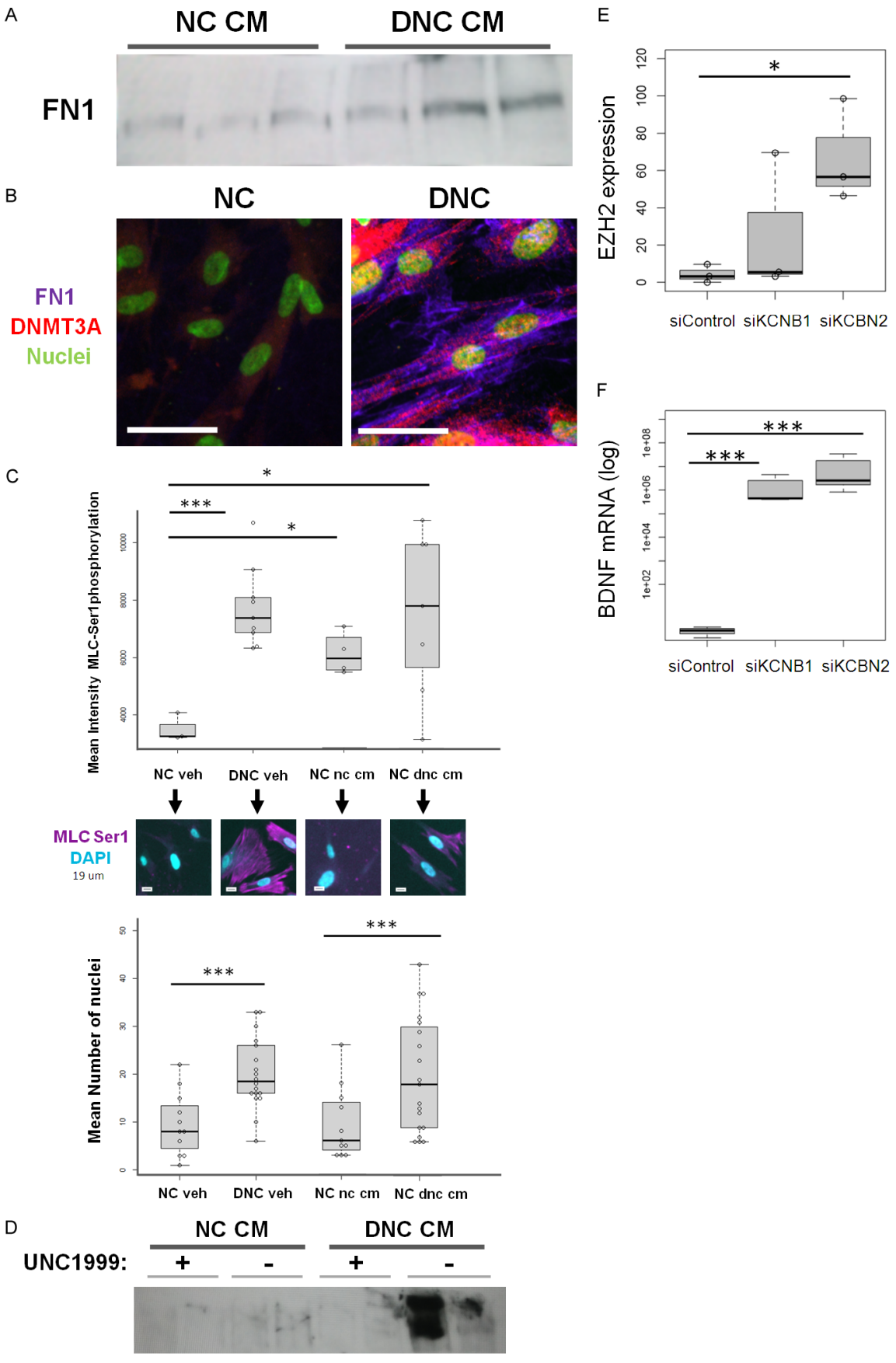
A
NC CM
DNC CM
FN1
B
NC
DNC
FN1
DNMT3A
Nuclei
C
Mean Intensity MLC-Ser1phosphorylation
NC veh
DNC veh
NC nc cm
NC dnc cm
MLC Ser1
DAPI
19 um
Mean Number of nuclei
D
NC CM
DNC CM
UNC1999:
E
EZH2 expression
siControl
siKCNB1
siKCBN2
F
BDNF mRNA (log)
siControl
siKCNB1
siKCBN2

Figure 4. Effects of conditioned media (CM) on cell phenotype. A. Western Blotting of FN1 from CM of cells plated on NC/DNC for 24 hours. The DNC-CM contained higher FN1 levels than the NC-CM. B. Immunofluorescent staining of DNMT3a and FN1 in bSMC plated on NC and DNC matrices, demonstrated increased expression of both DNMT3a and FN1 in the DNC matrix compared to the NC matrix. White bar for NC and DNC stains = 45 microns. C. Immunofluorescent staining for MLC-Ser1-P of SMC in 4 conditions: SMC plated on (1) NC (NC Veh); (2) DNC matrices (DNC Veh); (3) NC treated with NC-CM (NC recipient cells treated with CM from NC cells); or (4) NC treated with DNC-CM (NC recipient cells treated with CM from DNC cells). DNC Veh shows higher expression of MLC-Ser1-P in comparison to the NC Veh. MLC-Ser1-P expression also significantly increased in NC DNC-CM cells, suggesting that DNC-CM has a similar effect to DNC alone. However, there is slight recovery of MLC expression in NC NC-CM treatment cells, which contrasts with the NC Vehicle treatment. DNC Vehicle cells demonstrate a significant increase in cell number, which is also reflected in NC DNC-CM treatment cells. D. SMC plated with or without UNC1999 on NC or DNC produce conditioned media with differential FN1 content. Similar low levels of FN1 expression are produced by cells plated on NC, regardless of treatment (NC-CM). However, FN1 secretion is increased in cells plated on DNC (in the DNC-CM) but not when cells were treated with UNC1999, indicating a loss of FN1 secretion upon EZH2 suppression/loss of H3K27me3. E. SMC electroporated with siKCNB1 or 2, demonstrated increased expression of EZH2 after 24 hours culture, $P<0.05$. F. These same cells showed exponentially increased panBDNF expression in the siKCNB2 treatment vs. control, $^*P<0.005$.

We also examined if a major dysregulated gene during obstruction and COBD, BDNF, also changed in expression by siRNA KCNB2. The siRNA targeting both KCNB1 and 2 caused an increase in BDNF expression greater than 1000-fold, ***, $P<0.005$ using -ΔΔCt values (**Figure 4F**). ΔΔCt values were utilized as the logarithmic scale is more appropriate for assessing large differences in expression between groups. CTGF, another gene often co-regulated with BDNF was also upregulated by knockdown of KCNB2 (Supplementary Figure 4).

Discussion

H3K27me3 is a highly repressive epigenetic mark for cell-type specific gene expression[25]. Our results showed that H3K27me3 levels in the nucleus were globally increased by immunostaining in both PBO and COBD states. In the KCNB2 locus, PBO and COBD demonstrated higher levels of H3K27me3. *In vitro,* KCNB2 expression in bladder smooth muscle cells decreased on damaged matrix (DNC), which can be considered a cognate to the matrix environment of chronic obstructive bladder disease. This loss of KCNB2 was recovered by inhibiting H3K27 trimethylation (**Figure 3A-C**), demonstrating a functional role for EZH2 in down-regulation of KCNB2. Interestingly, there was a link between the downregulation of KCNB1/2 and upregulation of BDNF expression (**Figure 4F**), which we have previously shown to have increased levels of BDNF. EZH2 itself (**Figure 4E**) as well as CTGF (Supplementary Figure 4) were also upregulated by KCNB2 but not KCNB1 siRNA, suggesting that KCNB2 has an effect separate from KCNB1, with potential to regulate a network of genes.

Damaged matrix also elicited secretion of high levels of FN1 into the conditioned media, which was also deposited on SMC (**Figure 4A**, **4B**). This was consistent with the switch to a secretory type of SMC. The secreted factors of the conditioned media which included FN1 had multiple effects on SMC phenotype, including a rise in cell number and loss of contractile markers. FN1 may be just one of many secreted factors, but is known to have RGD epitopes and can elicit proliferation in bladder and other SMC [27-29]. Furthermore, the secretion of FN1 into the media was blocked by EZH2 inhibitor UNC1999 (**Figure 4D**). As FN1 in the bladder has not been highly studied, with much of the matrix focus on collagen expression. However, recent work by our lab showed that one of the most upregulated genes early in bladder obstruction is FN1 (Sidler Submitted, Biorxiv here: [30]). This work shows that FN1 dysregulation appears to continue on into chronic obstruction, and has an epigenetic underpinning at least in part through KCNB2 dysregulation by EZH2, thereby increasing the secretion of FN1 in bladder SMC. It will be of interest in future to examine what kind of secretory phenotype is being induced and further understand its epigenetic regulation.

While we focused on FN1 as the most highly upregulated matrix protein, other ECM proteins may be of interest to study in the future. In particular, Col4a1 and Col4a2 are upregulated in mouse (Sidler *et al.,* Submitted, please refer to BioRxiv [30]), consistent with work by Ekman *et al.*, 2013 [32], where the expression and distribution of collagen 4 was altered. Other collagens were also upregulated in our mouse dataset (e.g., Col7a1, Col17a1 and Col24a1). Col7a1 and Col24a1 can form triple helical fibrils, while

Col17a1 is a transmembrane protein that links intracellular elements to the ECM. As collagen types 4, 7 and 24 are secreted, they could be examined for effects on SMC phenotype and function in future studies.

However, it is important to note that inhibiting and activating H3K27 trimethylation had similar effects on calponin expression (**Figure 3**). This highlights the complexity of using broad epigenetic inhibitors as they can affect multiple groups of regulators in different ways yet end up with similar effects on phenotype. In this particular case, however, we can see that KCNB2 itself appears to be a crucial regulator of EZH2 activity and BDNF expression. This potential for reciprocal regulation opens up the possibility of a feedback loop whereby down-regulation of KCNB2 by EZH2 may also increase EZH2 expression, and in turn cause further decreases in KCNB2. Given the upregulation of FN1 by siRNA against KCNB2 (**Figure 2C**), this type of positive feedback may be important to identify in the development of long-lasting matrix changes in chronic bladder disease [4, 5, 31] which does not revert back easily despite release of the obstruction. Uncovering these positive regulation connections will open up potential beneficial therapies that arrest their continued activation.

Acknowledgements

This work was supported in part by the 2022 Urology Care Foundation Research Scholar Award Program and the AUA Northeastern Section (PY). The authors gratefully acknowledge funding from the Canadian Institutes of Health Research (DB).

Disclosure of conflict of interest

None.

Abbreviations

COBD, chronic obstructive bladder disease, which results from PBO in the persistent phase after de-obstruction; DNC, Disorganized collagen matrix; NC, Native collagen matrix; PBO, Partial bladder outlet obstruction; SMC, smooth muscle cells.

Address correspondence to: Karen J Aitken and Darius Bägli, The Hospital for Sick Children, Toronto, Ontario, Canada. E-mail: karen.aitken@alumni.utoronto.ca (KJA); darius.bagli@sickkids.ca (DB)

References

[1] Jarvis T, Chughtai B and Kaplan S. Bladder outlet obstruction and BPH. Curr Bladder Dysfunct Rep 2014; 9: 372-378.

[2] Vale L, Jesus F, Marcelissen T, Rieken M, Geavlete B, Rahnama'i MS, Martens F, Cruz F and Antunes-Lopes T; EAU Young Academic Urologists Functional Urology Working Group. Pathophysiological mechanisms in detrusor underactivity: novel experimental findings. Low Urin Tract Symptoms 2019; 11: 92-98.

[3] Lin WY, Wu CF and Chen CS. Partial bladder outlet obstruction: bladder dysfunction and related issues in animal studies. Urol Sci 2010; 21: 70-74.

[4] Fusco F, Creta M, De Nunzio C, Iacovelli V, Mangiapia F, Li Marzi V and Finazzi Agrò E. Progressive bladder remodeling due to bladder outlet obstruction: a systematic review of morphological and molecular evidences in humans. BMC Urol 2018; 18: 15.

[5] Mirone V, Imbimbo C, Longo N and Fusco F. The detrusor muscle: an innocent victim of bladder outlet obstruction. Eur Urol 2007; 51: 57-66.

[6] Andersson KE and Arner A. Urinary bladder contraction and relaxation: physiology and pathophysiology. Physiol Rev 2004; 84: 935-986.

[7] Hennus PM, van der Heijden GJ, Bosch JL, de Jong TP and de Kort LM. A systematic review on renal and bladder dysfunction after endoscopic treatment of infravesical obstruction in boys. PLoS One 2012; 7: e44663.

[8] Sidler M, Aitken KJ, Jiang JX, Sotiropoulos C, Aggarwal P, Anees A, Chong C, Siebenaller A, Thanabalasingam T, White JM, Choufani S, Weksberg R, Sangiorgi B, Wrana J, Delgado-Olguín P and Bägli DJ. DNA methylation and the YAP/WWTR1 pathway prevent pathologic remodeling during bladder obstruction by limiting expression of BDNF. Am J Pathol 2018; 188: 2177-2194.

[9] Jiang JX, Aitken KJ, Sotiropoulos C, Kirwan T, Panchal T, Zhang N, Pu S, Wodak S, Tolg C and Bägli DJ. Phenotypic switching induced by damaged matrix is associated with DNA methyltransferase 3A (DNMT3A) activity and nuclear localization in smooth muscle cells (SMC). PLoS One 2013; 8: e69089.

[10] Sidler M, Aitken KJ, Jiang JX, Yadav P, Lloyd E, Ibrahim M, Choufani S, Weksberg R and Bägli D. Inhibition of DNA methylation during chronic obstructive bladder disease (COBD) improves function, pathology and expression. Sci Rep 2021; 11: 17307.

[11] Pérez-Novo CA and Bachert C. DNA methylation, bacteria and airway inflammation: latest insights. Curr Opin Allergy Clin Immunol 2015; 15: 27-32.

[12] Tolg C, Sabha N, Cortese R, Panchal T, Ahsan A, Soliman A, Aitken KJ, Petronis A and Bägli DJ. Uropathogenic E. coli infection provokes epigenetic downregulation of CDKN2A (p16-INK4A) in uroepithelial cells. Lab Invest 2011; 91: 825-836.
[13] Ting K, Aitken KJ, Penna F, Samiei AN, Sidler M, Jiang JX, Ibrahim F, Tolg C, Delgado-Olguín P, Rosenblum N and Bägli DJ. Uropathogenic E. coli (UPEC) infection induces proliferation through enhancer of zeste homologue 2 (EZH2). PLoS One 2016; 11: e0149118.
[14] Guo C, Balsara ZR, Hill WG and Li X. Stage- and subunit-specific functions of polycomb repressive complex 2 in bladder urothelial formation and regeneration. Development 2017; 144: 400-408.
[15] Chu L, Qu Y, An Y, Hou L, Li J, Li W, Fan G, Song BL, Li E, Zhang L and Qi W. Induction of senescence-associated secretory phenotype underlies the therapeutic efficacy of PRC2 inhibition in cancer. Cell Death Dis 2022; 13: 155.
[16] Serresi M, Gargiulo G, Proost N, Siteur B, Cesaroni M, Koppens M, Xie H, Sutherland KD, Hulsman D, Citterio E, Orkin S, Berns A and van Lohuizen M. Polycomb repressive complex 2 is a barrier to KRAS-driven inflammation and epithelial-mesenchymal transition in non-small-cell lung cancer. Cancer Cell 2016; 29: 17-31.
[17] Thomas AA, Feng B and Chakrabarti S. ANRIL regulates production of extracellular matrix proteins and vasoactive factors in diabetic complications. Am J Physiol Endocrinol Metab 2018; 314: E191-E200.
[18] Schröder A, Aitken KJ, Jiang JX, Sidler M, Tolg C, Siebenaller A, Jeffrey N, Kirwan T, Leslie B, Wu C, Weksberg R, Olguin PD and Bägli DJ. Persistent myopathy despite release of partial obstruction: in vivo reversal of dysfunction and transcriptional responses using rapamycin. FASEB J 2020; 34: 3594-3615.
[19] Aitken KJ and Bägli DJ. The bladder extracellular matrix. Part I: architecture, development and disease. Nat Rev Urol 2009; 6: 596-611.
[20] Malmqvist U, Arner A and Uvelius B. Contractile and cytoskeletal proteins in smooth muscle during hypertrophy and its reversal. Am J Physiol 1991; 260: C1085-C1093.
[21] Guven A, Lin WY, Leggett RE, Kogan BA, Levin RM and Mannikarottu A. Effect of aging on the response of biochemical markers in the rabbit subjected to short-term partial bladder obstruction. Mol Cell Biochem 2007; 306: 213-219.
[22] Zhu B, Daoud F, Zeng S, Matic L, Hedin U, Uvelius B, Rippe C, Albinsson S and Swärd K. Antagonistic relationship between the unfolded protein response and myocardin-driven transcription in smooth muscle. J Cell Physiol 2020; 235: 7370-7382.
[23] DiSanto ME, Stein R, Chang S, Hypolite JA, Zheng Y, Zderic S, Wein AJ and Chacko S. Alteration in expression of myosin isoforms in detrusor smooth muscle following bladder outlet obstruction. Am J Physiol Cell Physiol 2003; 285: C1397-C1410.
[24] Herz DB, Aitken K and Bägli DJ. Collagen directly stimulates bladder smooth muscle cell growth in vitro: regulation by extracellular regulated mitogen activated protein kinase. J Urol 2003; 170: 2072-2076.
[25] Palomino-Morales R, Perales S, Torres C, Linares A and Alejandre MJ. Cholesterol loading in vivo and in vitro alters extracellular matrix proteins production in smooth muscle cells. Eur J Lipid Sci Technol 2016; 118: 1317-1325.
[26] Sakata N, Meng J and Takebayashi S. Effects of advanced glycation end-products on the proliferation and fibronectin production of smooth muscle cells. J Atheroscler Thromb 2000; 7: 169-176.
[27] Liu N, Xue Y, Tang J, Zhang M, Ren X and Fu J. The dynamic change of phenotypic markers of smooth muscle cells in an animal model of cerebral small vessel disease. Microvasc Res 2021; 133: 104061.
[28] Jain M, Dhanesha N, Doddapattar P, Chorawala MR, Nayak MK, Cornelissen A, Guo L, Finn AV, Lentz SR and Chauhan AK. Smooth muscle cell-specific fibronectin-EDA mediates phenotypic switching and neointimal hyperplasia. J Clin Invest 2020; 130: 295-314.
[29] Upadhyay J, Aitken KJ, Damdar C, Bolduc S and Bägli DJ. Integrins expressed with bladder extracellular matrix after stretch injury in vivo mediate bladder smooth muscle cell growth in vitro. J Urol 2003; 169: 750-755.
[30] Sidler M, Aitken KJ, Ahmed A, Jiang JX, Yadav P, Davani D, Huang R, Weksberg R and Bagli DJ. Human - murine concordance of molecular signatures in nerve-sparing murine partial bladder outlet obstruction (NeMO). bioRxiv 2021.09.15.460523.
[31] Mirone V, Imbimbo C, Sessa G, Palmieri A, Longo N, Granata AM and Fusco F. Correlation between detrusor collagen content and urinary symptoms in patients with prostatic obstruction. J Urol 2004; 172: 1386-1389.
[32] Ekman M, Bhattachariya A, Dahan D, Uvelius B, Albinsson S and Swärd K. MiR-29 repression in bladder outlet obstruction contributes to matrix remodeling and altered stiffness. PLoS One 2013; 8: e82308.

Supplementary materials: Statistical process in R 'stats' for determining significance of the data.

Determine significance of data by analysis of variance with linear model

```
lm_fit<- lm (y~x, data = the_data)
res.aov<-anova (lm_fit)
aov_residuals <- residuals (object = res.aov)

##Test for normality: Shapiro-Wilk's test
shapiro.test (x = aov_residuals)

# test for equal variance
bartlett.test (y~x, data = the_data)

# for unequal variances, use Welch's t.test:
test.welch (y~x, data = the_data)

#if normality and variance are normal, use regular Student's t.test:
t.test (y~x, data = the_data, var.equal=TRUE, conf.level=0.95)

#if variance not homogenous, use Kruskal-Wilks test
kruskal.test(y~x, data = the_data)
```

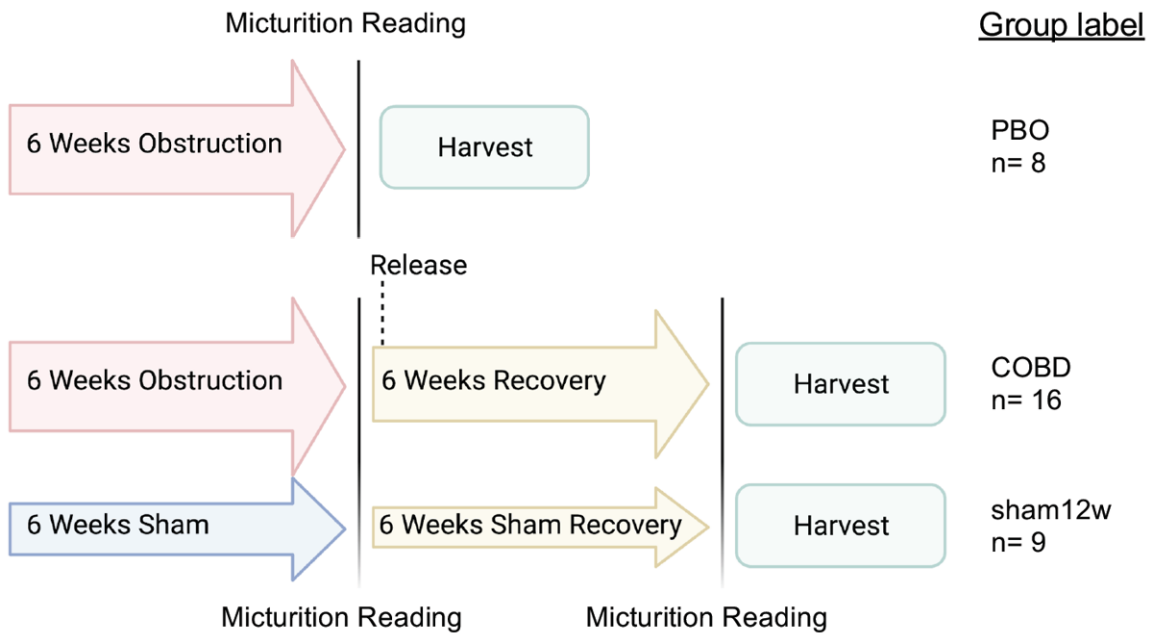

Supplementary Figure 1. Schematic of obstruction and de-obstruction treatments, and bladder physiology readings in PBO, COBD and Sham rats [8, 10]. These models provided the archival tissues for DNA ChIP analysis and immunostaining.

Supplementary Table 1. Non-invasive bladder functional monitoring from a set of archival samples of de-obstructed and obstructed [8, 10]

Surgery type	Total no. voids	No. small/ total voids	Residual Vol (mL)	Bladder mass (mg)	Maximum voiding fraction	Mean voiding fraction	Mean VV (mL)	Bladder Capacity (mL)
sham	9 ± 1.166	0.18 ± 0.095	0.09 ± 0.037	110 ± 4.3	0.87 ± 0.054	0.50 ± 0.066	0.56 ± 0.11	0.94 ± 0.12
PBO	12.5 ± 3.8	0.29 ± 0.18*	5.42 ± 1.3**	430 ± 77**	0.21 ± 0.080**	0.13 ± 0.06**	0.67 ± 0.23	6.6 ± 1.2**
COBD	7 ± 0.894	0.17 ± 0.068	0.12 ± 0.021	180 ± 9.5**	0.82 ± 0.16	0.40 ± 0.048*	0.73 ± 0.086	2.0 ± 0.28*

*, p<0.05; **, p<0.01, student's t-test.

Supplementary Table 2. RT-PCR and ChIP genomic KCNB2 Primers, sequence or reference and annealing temperatures

Primer name	Sequence (5'-3')	Temperature
ChIP rat KCNB2 350 bp upstream for	CCCCAGCTTTGGGGTGTAAT	65
ChIP rat KCNB2 350 bp upstream rev	ACACGCAATGTTTCGACTGC	
ChIP rat KCNB2 56 bp upstream for	CCTGACATATGGCCACGGAG	65
ChIP rat KCNB2 56 bp upstream rev	TAGCCGCCAACACAGAAAGG	
ChIP rat BDNF for	CCCTGGAACGGAATTCTTCT	65
ChIP rat BDNF rev	GATACCTCCTCTGCCTCGAA	
mRNA hu FN1 for	GGTGACACTTATGAGCGTCCTAAA	60
mRNA hu FN1 rev	AACATGTAACCACCAGTCTCATGTG	

Primers and conditions for human EZH2, human panBDNF, human CTGF, human B2M, human RPL13, human HPRT, human UBC, rat RPL32, rat HPRT, rat B2M and rat beta-actin were previously published with Sidler *et al.*, 2018, 2021 [8, 10] and Ting *et al.*, 2016 [13].

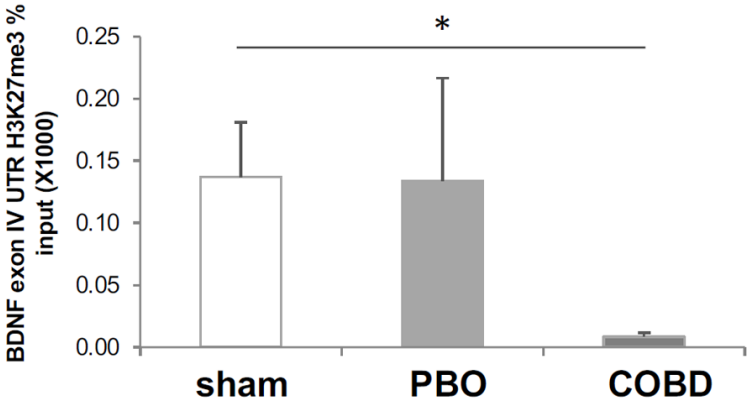

Supplementary Figure 2. Percentage input analysis of BDNF Exon IV Transcription Start Site (TSS) region H3K27me3 expression profile. PBO and Sham tissues show similar expression of H3K27me3 in BDNF Exon IV TSS. However, COBD shows a significant decrease in H3K27me3 expression levels, indicating a lack of repression of BDNF in COBD tissues. This also correlates function and expression of BDNF.

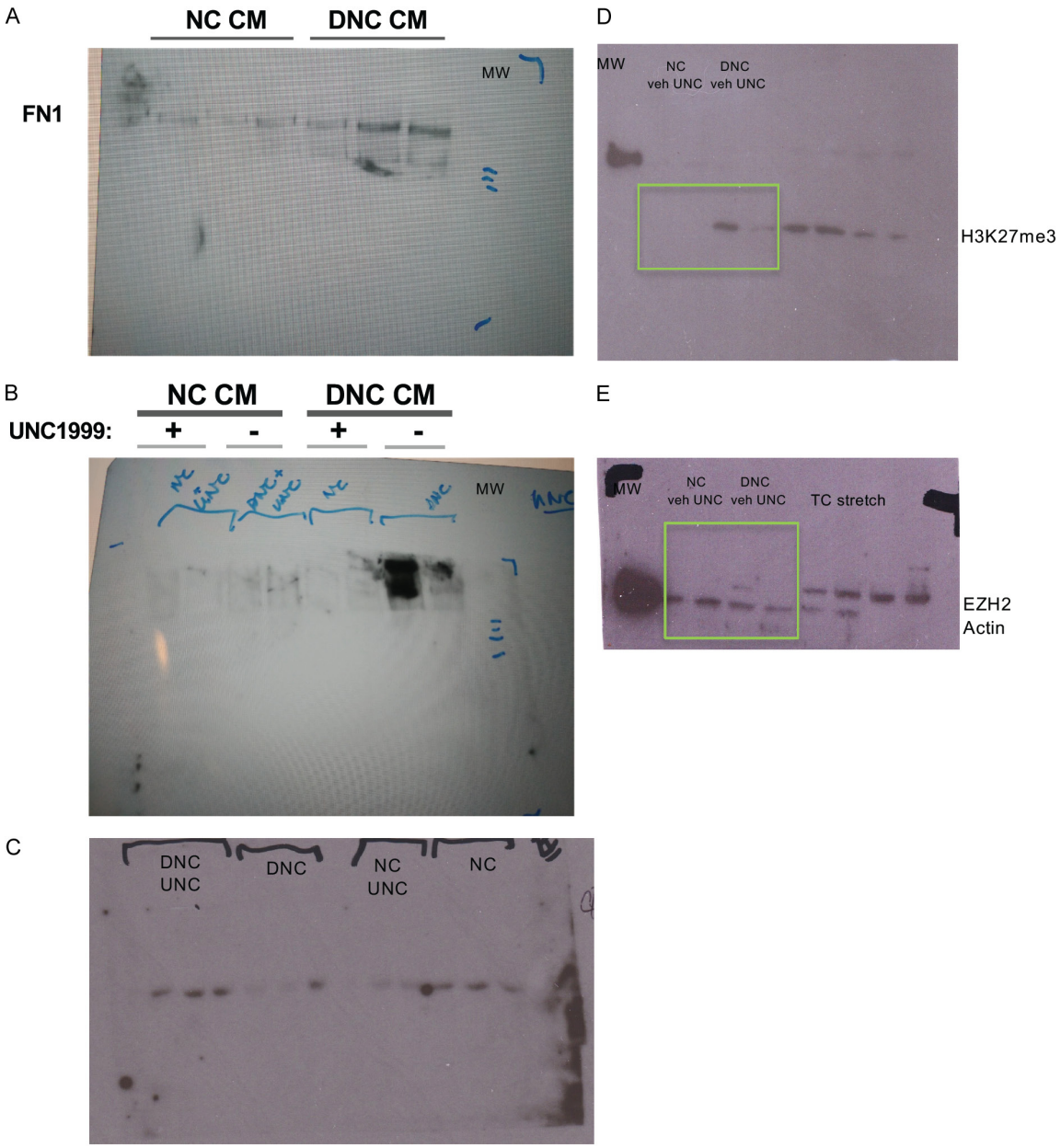

Supplementary Figure 3. Complete autoradiographs for Western blots for **Figures 3A**, **4A** and **4D**. A. Western Blotting of FN1 from CM of cells plated on NC/DNC for 24 hours. The DNC-CM contained higher FN1 levels than the NC-CM. B. SMC plated with or without UNC1999 on NC or DNC produce conditioned media with differential FN1 content. Similar low levels of FN1 expression are produced by cells plated on NC, regardless of treatment (NC-CM). FN1 secretion is increased in cells plated on DNC (in the DNC-CM) but not when cells were treated with UNC1999, indicating a loss of FN1 secretion upon EZH2 suppression/loss of H3K27me3. C. KCNB2 expression in replicates with and without UNC1999 treatment on NC vs. DNC substrates. D. A replicate from C showing H3K27me3 loss with UNC1999 treatment on DNC. E. A replicate from C with EZH2 increased on DNC vs. NC vs. pan-actin in lower lane. The TC (tissue culture) and stretched samples on this gel were not included in this paper. MW = colorimetric molecular weight lane. The MW lane showed some background reactivity at one MW marker.

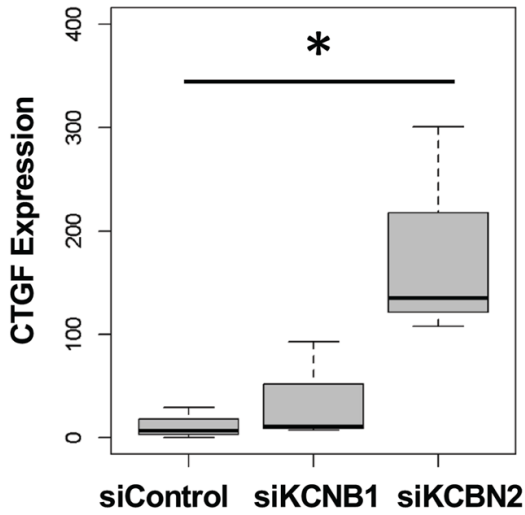

Supplementary Figure 4. CTGF expression in KCNB2 depleted (by siRNA) cells was significantly upregulated, $P<0.01$ on delta-delta ct values, as the logarithmic scale is more appropriate for large differences in expression.